Electronic response in a one-dimensional nonlinear lattice

Yi Wan and C. M. Soukoulis
Ames Laboratory–U.S. Department of Energy and Department of Physics, Iowa State University, Ames, Iowa 50011-3020
(Received 18 May 1989)

We study electronic response in a one-dimensional nonlinear lattice in terms of a transmission problem where the nonlinear Schrödinger equation of the tight-binding form is considered to describe the motion of the electrons. We introduce an area-preserving nonlinear mapping for the transmission problem. We then analyze this mapping in the context of nonlinear dynamical theory, and discuss the results in terms of physical quantities describing the transmission process. We show a "phase diagram" in terms of the electronic energy and nonlinear coupling constant for the solutions which contribute to the transmission. We also calculate the transmission coefficients as functions of the nonlinear coupling constant. Our results demonstrate how interesting properties, such as multistability and noise, occur in the electronic response of our problem. Several physical models involving electronic or optical processes are considered as systems that might be relevant to our study.

I. INTRODUCTION

The one-dimensional nonlinear Schrödinger equation has appeared in a number of theoretical models in condensed-matter physics. These include, among others, the Holstein molecular-crystal chain[1] and adiabatic theories involving short-range electron-phonon interaction in quasi-one-dimensional systems in general,[2] nonlinear-optical responses in superlattices formed by dielectric or magnetic slabs,[3] and, most recently, the mean-field theory of a periodic array of twinning planes in the high-T_c superconducting oxides.[4] The existence of fundamental periodic modulations in these models often leads to a one-dimensional time-independent nonlinear Schrödinger equation of the tight-binding form:

$$-\psi_{n-1}-\psi_{n+1}-\lambda|\psi_n|^2\psi_n=E\psi_n\ , \tag{1}$$

where E and λ are the energy of the wave and the nonlinear coupling constant, respectively, and ψ_n can be the electron wave function, the effective electromagnetic field, or the superconductivity order parameter at the nth site of the lattice (superlattice). Typically, in search for solutions, the continuum approximation is applied to Eq. (1), and the resulting differential equation can be integrated. The solutions are then matched to the boundary conditions of the problem. Such a procedure is justified in cases where the solutions are slowly varying functions in space, on the scale of the lattice constant. However, there are circumstances in which the interplay of the effects of nonlinearity and periodic modulation has physical significance, such as pinning of the field by the lattice.[5] On the other hand, the discrete nonlinear Schrödinger equation [Eq. (1)] has the form of a nonlinear dynamical mapping, with n playing the role of discrete time. More precisely, it belongs to the class of area-preserving nonlinear mappings on the Poincaré surface of section describing the nonlinear dynamics of Hamiltonian systems. It is well known that such nonlinear mappings can have rich and complex behavior, due to their nonintegrable character.[6–13] Thus it is interesting to study, in simple physical systems, the consequence of nonintegrable nonlinear dynamics. We have studied elsewhere[14] the properties of Eq. (1) in both real and complex domains, using nonlinear dynamical methods, and have discussed their physical implications for an infinite lattice chain. Here we consider the problem of transmission through a one-dimensional nonlinear lattice chain of finite length. Specifically, we consider a finite nonlinear sample embedded in an infinite linear lattice chain, and electrons in the linear part of the system arriving at one end of the nonlinear sample, inducing excitations in the nonlinear medium (Fig. 1). Under certain conditions, such responses may be able to propagate through the nonlinear sample and emerge as a transmitted wave. After the process reached a static limit, the resulting stationary electron wave function in the nonlinear medium can be described by a time-independent nonlinear Schrödinger equation in the one-electron picture. Assuming the linear medium is described by the same tight-binding Schrödinger equation with $\lambda=0$, so that wave function there takes the form of a Bloch wave, and considering an incident wave coming from the left towards the nonlinear sample extending over N lattice sites, we define our transmission problem as the following (see Fig. 1):

$$\psi_n=R_0e^{ikn}+R_1e^{-ikn},\quad n\le 0 \tag{2a}$$

$$-\psi_{n+1}-\psi_{n-1}-\lambda|\psi_n|^2\psi_n=E\psi_n,\quad 0<n\le N \tag{2b}$$

$$\psi_n=Te^{ikn},\quad n>N\ . \tag{2c}$$

In Eqs. (2) we require $|R_0|^2=|R_1|^2+T^2$ to satisfy the conservation of probability current and choose the overall constant phase for the wave functions so that T is real.

We first explain the physical meaning of Eqs. (2) and our strategy for solving it. For the typical physical model

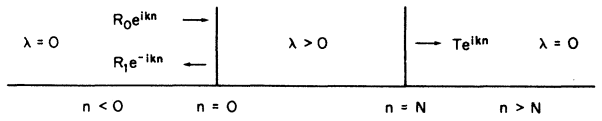

FIG. 1. Nonlinear transmission as defined by Eq. (2). The nonlinear medium ($\lambda > 0$) extends from $n = 0$ to $n = N$. There are incoming and reflected waves in the linear medium ($\lambda = 0$) to the left of the nonlinear sample ($n < 0$), whereas only the outgoing wave exists on the other side ($n > N$) of the nonlinear sample.

related to the nonlinear sample, we mention the large-polaron regime of the Holstein molecular-crystal chain,[1] where ψ_n represents the wave function of a single excess electron at the Fermi level E, and the cubic nonlinear term in Eq. (1), $\lambda|\psi_n|^2\psi_n$, originates from the static short-range electron-phonon interaction. It has been shown[1] that the ground state for the electron is in the form of localized polaron with energy in the gap of the corresponding decoupled system, and there are an infinite hierarchy of excited states above the ground state. These excitations can be coupled to the incident electron and hence contribute to the transmission process. We also note that the Holstein model can equally describe an excess hole in the molecular-crystal chain, provided λ is negative and that E and k refer to the energy and wave vector of the hole, respectively. Thus, we will restrict our study to the electron case only, i.e., $\lambda > 0$. The linear transmission problem [Eqs. (2) with $\lambda = 0$], even in the presence of random potentials, is well understood. The transmission coefficient $t = T^2/|R_0|^2$ vanishes, except for E in the energy band, i.e, $-2 \le E \le 2$, where $E = -2\cos k$ and k is the Bloch wave vector. In order to probe the nonlinear response for all possible energies in our model, we allow E to vary outside $[-2,2]$. This might be realized if we consider proper interface structures between the nonlinear sample and the linear leads, similar to that commonly adopted for metal-semiconductor interfaces.[15,16] The Fermi level E is then determined by the electron reservoir in the metal leads. However, in writing Eqs. (2) we have ignored for simplicity the regions dominated by space-charge fluctuations and surface states, as well as the associated effects such as band bending. Alternatively, one may suggest that there exists near the interface a linear region of a length small compared to the nonlinear sample, covering the space-charge extension, and the linear transfer-matrix can be used to move into the nonlinear region. This will not change the results qualitatively. With these considerations, one should choose independently the values of E and k in Eqs. (2). However, we restrict ourselves to the following two cases, according to whether $|E| \le 2$: (a) $E = -2\cos k$ for $-2 \le E \le 2$, and (b) for $E < -2$, a fixed value for the wave vector is used, namely $k = 2\pi/100$. It will be clear that the two cases represent two different regimes of the transmission problem, while (b) is particularly interesting since the transmission there is due entirely to the nonlinearity and its nature is truly nonperturbative (see discussions in Sec. III).

In the next section we derive a nonlinear mapping for the transmission problem and study its properties in the context of nonlinear dynamics. This provides us with information about the wave functions in the nonlinear sample and the relationship between the intensities of the incident wave $|R_0|^2$ and the transmitted wave T^2, i.e., the nonlinear response, as well as their dependence on the parameters E, k, and λ. As will be shown later, ψ_n, for $0 < n < N$, can be uniquely determined by the output Te^{ikn}, $n \ge N$, rather than by the input R_0. The overall behavior of the transmission can be summarized in terms of a "phase diagram" on the $(E, \lambda T^2)$ plane (see Fig. 2 and discussions in Sec. III), where a sharp and complex-structured boundary is seen to separate the shaded region corresponding to the bounded wave functions in the nonlinear sample, contributing to transmission, from that of diverging wave functions (i.e., *infinite input*). A special case of such a "phase diagram," with $-2 \le E \le 2$, was first discovered by Delyon and co-workers.[17] By introducing a nonlinear dynamical mapping for the complex wave functions, we are able to study the "phase diagram" and the associated structures in the transmission coefficient t. Moreover, we found chaotic behavior of the electronic states (as a direct consequence of the nonintegrability of the nonlinear mapping), contrary to the conclusions of the previous authors.[17,18] These detailed results and their implications are presented and discussed in Sec. III.

II. NONLINEAR DYNAMICAL MAPPING ON THE PLANE

Writing $\psi_n = x_n + iy_n$, Eq. (1) becomes

$$-x_{n+1} - x_{n-1} - \lambda(x_n^2 + y_n^2)x_n = Ex_n \ , \tag{3a}$$

$$-y_{n+1} - y_{n-1} - \lambda(x_n^2 + y_n^2)y_n = Ey_n \ . \tag{3b}$$

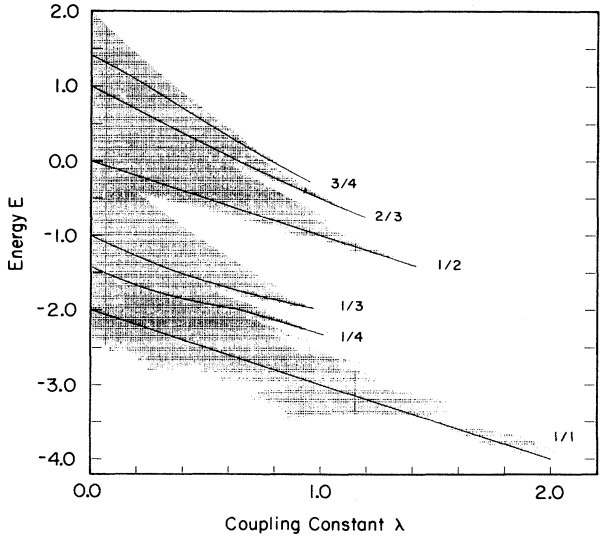

FIG. 2. "Phase diagram" of energy E vs the nonlinear strength λT^2, showing transmitting (shaded) and nontransmitting (unshaded) regimes of Eqs. (2). See discussion in Sec. III.

Equations (3) contains two coupled second-order difference equations and represents a four-dimensional nonlinear mapping in the phase space $(x_{n-1}, x_n, y_{n-1}, y_n)$. A particular problem that might arise for such a nonlinear system involves the so-called Arnold diffusion,[7-9] which is known to exist, in general, in nonlinear dynamical mappings with degrees of freedom greater than two. As a consequence, one cannot guarantee the existence of a particular bounded state (x_n, y_n) over arbitrary distance in the nonlinear medium. However, it can be shown that, because of the conservation of probability current required in our problem, this four-dimensional mapping can be reduced to a two-dimensional one, and the possibility of the Arnold diffusion can be ruled out.

In order to derive the reduced mapping, we write the wave function and Eqs. (3) in polar coordinates: $\psi_n = r_n e^{i\theta_n}$ and

$$r_{n+1}\cos(\Delta\theta_{n+1}) + r_{n-1}\cos(\Delta\theta_n) = 2f(r_n) , \tag{4a}$$

$$r_{n+1}\sin(\Delta\theta_{n+1}) - r_{n-1}\sin(\Delta\theta_n) = 0 , \tag{4b}$$

where $\Delta\theta_n = \theta_n - \theta_{n-1}$ and $f(r) = -\frac{1}{2}r(\lambda r^2 + E)$. The second equation defines an integral of motion for Eqs. (4):

$$J \equiv r_n r_{n-1}\sin(\Delta\theta_n) , \tag{5}$$

which has the physical meaning of probability current. Following Bountis and co-workers in their study[19] of a model for colliding proton beams in the storage ring, we introduce new variables:

$$\begin{bmatrix} u_n \\ v_n \end{bmatrix} = \begin{bmatrix} r_n^2 \\ J\cot(\Delta\theta_n) \end{bmatrix} . \tag{6}$$

We obtain from Eq. (5) and Eq. (4a) the reduced mapping S:

$$S: \quad u_{n-1} = \frac{1}{u_n}(v_n^2 + J^2) , \tag{7a}$$

$$v_{n-1} = -v_n - u_{n-1}(u_{n-1} + E) , \tag{7b}$$

where its variables have been scaled by the nonlinear coupling constant λ: $(u,v) \to (\lambda u, \lambda v)$, and λ is absorbed into J: $J \to \lambda J$. Besides E, the only other parameter in mapping S is the current J which describes the strength of the nonlinearity and can be determined from λ and the output of the transmission problem. The mapping S is related to the transmission problem as follows. From the wave functions at the boundary of the nonlinear sample, namely ψ_N and ψ_{N+1}, one finds immediately r_N, r_{N+1}, θ_N, and θ_{N+1}. Using Eqs. (5) and (6), J can be determined from u_N, u_{N+1}, v_{N+1}, and λ, while v_N is obtained from Eq. (7b). (u_N, v_N) is then used to initiate the iterations of S. Conversely, having obtained a series (u_n, v_n), one immediately has r_n and $\Delta\theta_n$ in $[0,\pi]$ if $J > 0$ (or in $[\pi, 2\pi]$ if $J < 0$): thus $\theta_n = -\sum_{m=n}^{N}\Delta\theta_{m+1}$. This procedure enables us to study the wave functions in the nonlinear medium in terms of the (bounded) orbits of mapping S on the (u,v) plane, which is the Poincaré surface of section of the corresponding nonlinear dynamical system (with n playing the role of discrete time). For the special case $J = 0$, we use Eqs. (3) directly, which is now decoupled and becomes the nonlinear Schrödinger equation in the real domain, which we have studied elsewhere.[14]

It can be shown that the mapping S is equivalent topologically to an area-preserving mapping. Indeed, S preserves the local measure in the coordinates $(\ln u_n, v_n)$. An important property of S is its reversibility, which we now discuss. By writing $S = S_2 S_1$, we factorize S into involutions S_1 and S_2:

$$S_1: \quad u' = \frac{1}{u}(v^2 + J^2) , \tag{8a}$$

$$v' = v ; \tag{8b}$$

$$S_2: \quad u' = u , \tag{8c}$$

$$v' = -v - u(u + E) . \tag{8d}$$

S_1 and S_2 satisfy $S_1^2 = S_2^2 = 1$, so that $S^{-1} = S_1 S_2$. The reversibility is evident in that Eq. (1) does not depend explicitly on n. Geometrically, the mapping S_1 has the effect of "inversion" along the u axis about the $(u > 0)$ branch of the hyperbola $u^2 - v^2 = J^2$, and S_2 represents a reflection about the parabola $v = -\frac{1}{2}u(u + E)$ along the v axis (cf. Fig. 3). The two curves $u = (v^2 + J^2)^{1/2}$ and $v = -\frac{1}{2}u(u + E)$ are the symmetry lines of S_1 and S_2, respectively, since each is actually formed by the set of fixed points of the corresponding mapping.

The orbits generated by the mapping S on the (u,v) plane can be either bounded or divergent. Only the bounded orbits contribute to wave transmissions in our problem. The bounded orbits are further organized into a hierarchy of periodic orbits of different periods, due to general theorems of Poincaré and of Birkhoff and the Kolmogorov-Arnold-Moser (KAM) theorem.[7] Each stable periodic orbit is surrounded by higher-order periodic and quasi periodic orbits, whereas around the unstable periodic orbits there are locally chaotic orbits. The stability of a periodic orbit of period q is determined

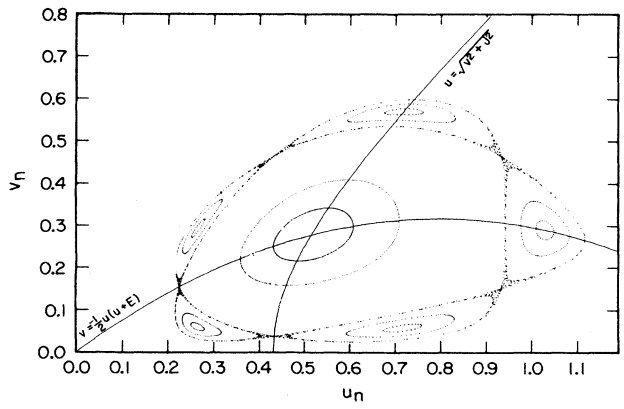

FIG. 3. Period-5 elliptic and hyperbolic orbits at $E = -1.598$ with their surrounding quasiperiodic and chaotic orbits on the (u,v) plane. The solid lines are part of the symmetry lines of mapping S_1 and S_2.

by its residue R, defined as $R=\frac{1}{4}[2-\mathrm{Tr}(\Pi_{n=1}^{q} DS^{(n)})]$, where $DS^{(n)}$ is the linearized mapping on the nth point of the orbit. A periodic orbit is stable (elliptic) when $0<R<1$, while it is unstable when $R<0$ (hyperbolic) or $R>1$ (hyperbolic with reflection). Notice that the periodic orbit and its residue are functions of the parameters in the mapping S. As an example, the period-1 periodic orbit is given by

$$u=-E-2\cos k \ , \tag{9a}$$

$$v=-(E+2\cos k)\cos k \ , \tag{9b}$$

with $R=1-(E/2)\cos k-2\cos^2 k$. We show in Fig. 3 the period-5 periodic orbit and the surrounding qausiperiodic and chaotic orbits. The presence of the chaotic orbit is closely related to the nonintegrable nature of the nonlinear dynamical mapping. Notice how the orbits are arranged about the two symmetry lines. In fact, the symmetry lines make it much easier to locate numerically a periodic orbit. Since the starting point of the iterations (u_N,v_N) is always on the symmetry line of S_1, i.e., $u_N=(v_N^2+J^2)^{1/2}$ (cf. Sec. III), it is sufficient to do a one-dimensional search for a periodic orbit of given period.

III. RESULTS AND DISCUSSIONS

Now we describe how the orbits of mapping S contribute to the wave transmission in our problem. At the right end of the nonlinear sample, the wave functions representing the transmitted wave are simply the Bloch waves [cf. Eqs. (2)]: $\psi_n=Te^{ikn}$, $n\geq N$. From Eqs. (4) and (5), we have $J=\lambda T^2\sin k$, $u_N=u_{N+1}=\lambda T^2$, and $v_{N+1}=\lambda T^2\cos k$ (we take $\lambda=1$ in all the numerical calculations), so that (u_N,v_N) is on the symmetry line of S_1. The "phase diagram" in Fig. 2 is plotted by choosing E, J, and (u_N,v_N) as discussed above, and by iterating the mapping S. If the iterations give a bounded orbit (a cutoff is used in the numerical procedure), then the point $(\lambda T^2,E)$ falls in the shaded region that we call the "stable zone"; otherwise it is in the unshaded region. We found that the boundary separating these two regions is insensitive to either the cutoff or the number of interactions as long as a moderate number of the order 10^2 is exceeded. The points $(\lambda T^2,E)$ corresponding to a particular stable periodic orbit form a curve extending from the vertical axis to a point on the boundary of the shaded region where the orbit loses its stability permanently. Several of the curves corresponding to the lowest-period orbits are shown in Fig. 2. However, there are infinite periodic orbits present and each is surrounded by quasiperiodic and chaotic orbits. These orbits, all together, produce the branches of the "phase diagram." There are also bifurcations from a periodic orbit whenever its residue reaches a rational number, producing higher classes of orbits which do not show in Fig. 2. Remarkably, for the area-preserving mappings, there are renormalization-group arguments[13] indicating that scaling relations exist among the classes of periodic orbits when the parameters approach limiting values. As a consequence, the boundary of the bounded orbits demonstrates fractal geometry.

The quantities of interest in the transmission problem are $|R_0|^2$ and t, which can be numerically calculated by iterating the mapping S with a specified E and k for various values of T ($\lambda=1$). The calculations are performed for the two typical cases indicated in Sec. I: one for $k=\pi/3$ and $E=-1$ and the other for $k=2\pi/100$ and $E=-2.01$, both with the same sample length $N=200$. The results are summarized in a series of plots in Figs. 4 and 5, which we now examine. Figures 4(a) and 4(b) show, on different scales, that the intensity of the incident wave, $|R_0|^2$, is a single-valued function of the transmitted intensity T^2. Figure 4(c) presents similar information in terms of the transmission coefficient t as a function of T^2. On the other hand, T^2 has a multivalued functional dependence on $|R_0|^2$, which is the source of bistability, or multistability, in general. Close examination of the plots reveals that such multivalued functional relations will result in resonances in the transmission, but there are also interrupting smooth or monotonic regions accompanied by narrow bursts of irregular variations, especially for large T. Eventually, they become very irregular and terminate when the wave function diverges and no transmission is possible. These seemingly complicated features can be organized and explained in light of the "phase diagrams" in Fig. 2 and the general structures of the bounded orbits. For fixed E and k in Fig. 2, T^2 can be in either the shaded region or unshaded region; consequently, there are total reflection gaps in the transmission region. Roughly speaking, when T^2 is deep inside the shaded region, the transmission variations are relatively smooth, while they become irregular as T^2 approaches the boundary of the shaded region.

Figure 4(d) establishes the connection between the transmission and the orbits on the $(\ln u,v)$ plane, where several low-period periodic orbits and surrounding quasiperiodic orbits are generated from values of T^2 in Fig. 4(a). Each of these orbits corresponds to a state in real space of the nonlinear sample, fluctuating like a charge-density wave. We should remark that among all orbits the periodic ones form a set of zero measure, so that almost all of the contributions to the transmission come from the bounded quasiperiodic or chaotic orbits. However, the behavior of quasiperiodic is determined by the periodic ones they surround. For instance, the innermost orbit in Fig. 4(d) represents one of the quasiperiodic orbits around the period-1 elliptic orbit (fixed point of mapping S) at $T^2=0.0139$ [cf. Eqs. (9) and Fig. 4(b)]. Such orbits are responsible for the part of transmission in Fig. 4(a) below the point $T^2\approx 0.45$. As T^2 increases, orbits of similar type with larger size are now contributing to the transmission, and $|R_0|^2$ or t would show similar smooth or resonant variations. This tendency continues as long as the quasiperiodic orbits remain in the basin of a particular periodic orbit. Similar behaviors are seen around $T^2=0.47$ and 0.71, coming from the orbits in the basins of the period-5 and period-4 elliptic orbits, respectively. However, when the relevant orbit switches between basins as T^2 is varied, one would expect the transmission variations to behave differently. Moreover, in the vicinity of the hyperbolic period orbits, such changes occur in a violent and chaotic way, producing the irregular variations in the transmission. The region occupied by chaotic

orbits grows wider as one moves away from the lowest-order elliptic orbit. In Fig. 4(d) the chaotic orbits originating from the period-4 hyperbolic orbits are evident, which give rise to the irregular "bursts" on the transmission bordering the region centered at $T^2=0.71$. Notice that there are still quasiperiodic orbits surrounding chaotic orbits. In fact, such quasiperiodic orbits exist up to the edges of the total reflection gap, and they prevent the local chaotic orbits from diverging.

The resonant behavior of the states in the nonlinear sample are shown in Fig. 4(e), where the probability density of the electron is plotted. All three states plotted

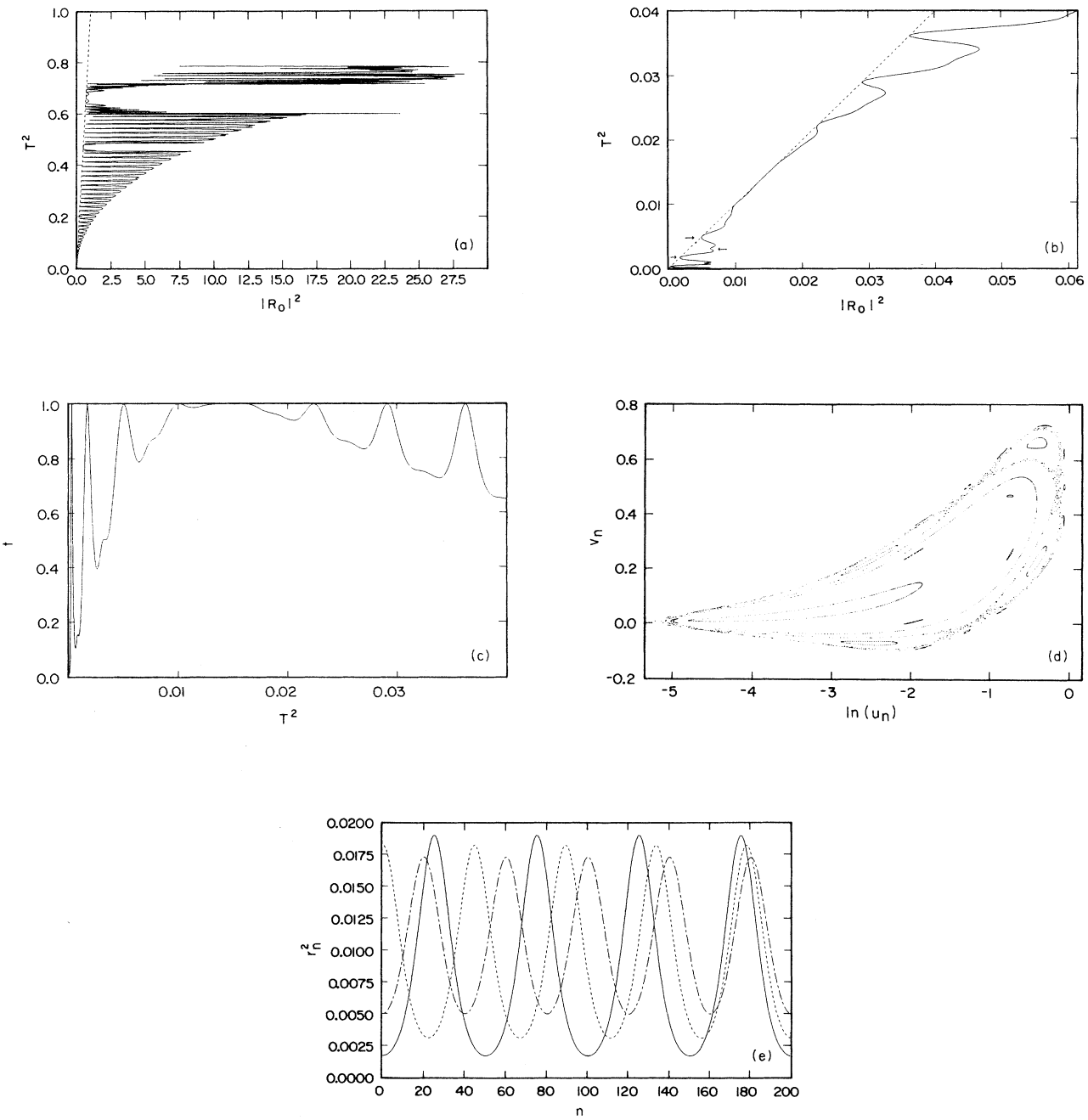

FIG. 4. (a) Transmitted intensity T^2 vs the incident intensity $|R_0|^2$ at $E=-2.01$. The dashed line corresponds to $T^2=|R_0|^2$, which describes the linear transmission. (b) Enlargement of the section around the origin in (a). (c) Transmission coefficient t vs T^2 for $E=-2.01$. T^2 has the same range as in (b). (d) Some of the orbits corresponding to values of T^2 in (a) on the $(\ln u, v)$ plane. (e) Probability density in the nonlinear sample r_n^2 as function of n at $E=-2.01$ and $T^2=1.7\times10^{-3}$ (——), 3.1×10^{-3} (— — —), and 5.0×10^{-3} (—·—·—·). These values of T^2 are also indicated by arrows in (b).

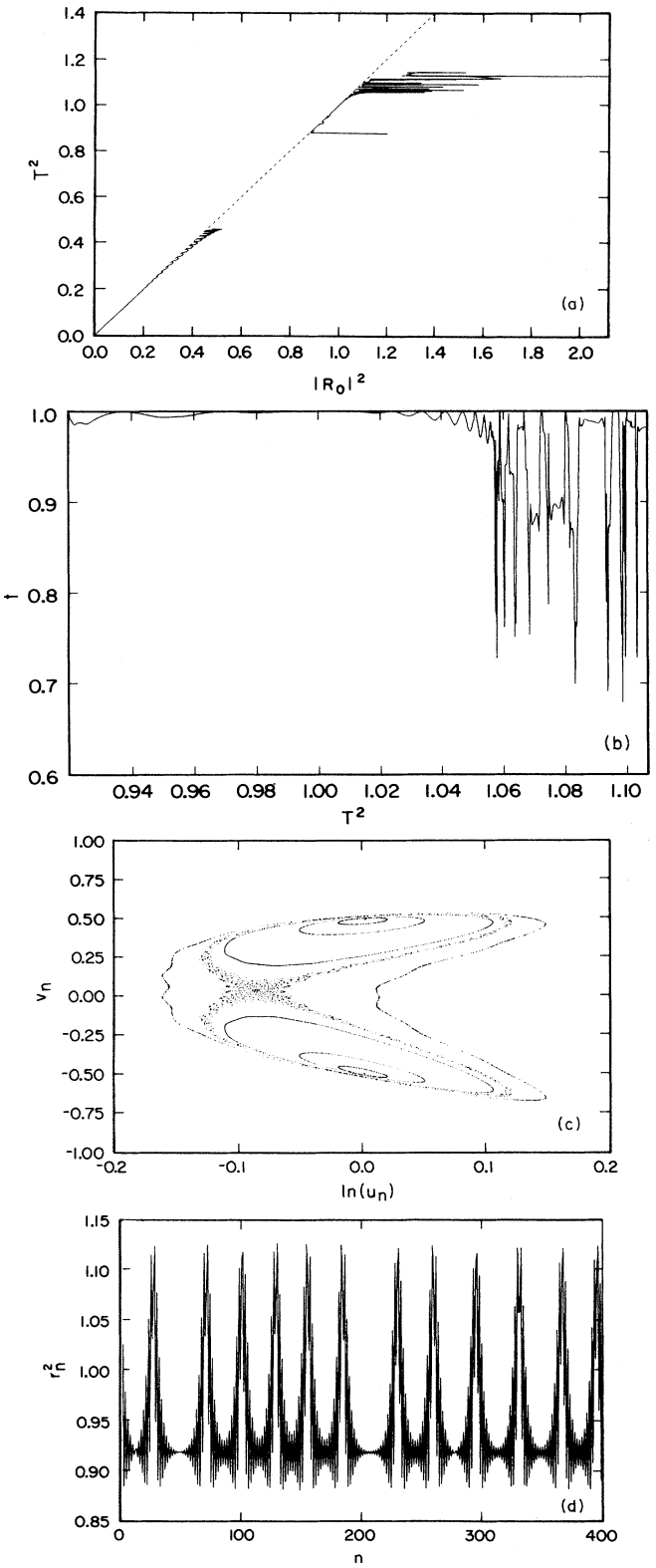

FIG. 5. (a) Same as Fig. 4(a), but for $E=-1.0$. The total reflection gap from $T^2=0.45$ to 0.92 can be seen. (b) Transmission coefficient t vs T^2 for $E=-1.0$. (c) Some of the orbits corresponding to values of T^2 in (b) on the $(\ln u, v)$ plane. (d) Similar to Fig. 4(e), but for $E=-1.0$ and $T^2=1.0593$, showing the chaotic orbit around the hyperbolic period-2 orbit in (c).

correspond to the quasiperiodic orbits around the period-1 elliptic orbit at $T^2=0.0139$, and their corresponding T^2 values are indicated in Fig. 4(b). Since the states have values of T^2 smaller than 0.0139, and the iterations all begin with $r_N^2=r_{N+1}^2=T^2$, their probability densities have minima at $n=N=200$. However, at the left end of the nonlinear sample, the intensity of the reflected wave is given by

$$|R_1|^2=\frac{1}{4\sin^2 k}[(u_0-u_N)+(u_1-u_{N+1}) -2(v_1-v_{N+1})\cos(k)]\geq 0 .$$

Thus, only the states that have an integral number of complete resonances inside the nonlinear sample can cause $|R_1|^2=0$, i.e., producing resonant transmission with $t=1$. We also see how the special nature of the transmission problem, i.e., that a relevant orbit is determined by the output rather than the input, and the nonlinearity-induced resonances give rise to the multistable property in the transmission. It is evident that as the sample length N is varied while the remaining parameters are unchanged, the condition for resonant transmission will be changed. This results in shifts of the resonant-transmission peaks on the t-versus-T^2 plot.

We now turn to Fig. 5, with E in the energy band of the corresponding linear sample. Comparing the plots in Fig. 5 with those in Fig. 4, we see that the two cases share the properties discussed above. However, important differences appear in the small-T^2 part of their $|R_0|^2$-versus-T^2 relations [note the resonant behavior in Fig. 4(b) as $T^2\to 0$; this behavior is absent in Fig. 5(a)]. The reason for this is that we adopted the relation $E=-2\cos k$ only for $-2<E<2$, so that the period-1 orbit has vanishing u [cf. Eqs. (9)], leading back to the linear case. In fact, its corresponding state is described by the Bloch waves, whereas for $E<-2$ Eqs. (9) indicate a finite-u, period-1 orbit. Hence, for the latter, decreasing T^2 from 0.0139 has a similar effect as increasing T, both carrying the orbits away from the period-1 elliptic orbit. Consequently, one enters the truly nonperturbative regime when E is below -2 such that the shaded region moves away from $T=0$ (this becomes visible when $E\leq -2.45$ in Fig. 2). There, a critical value of T or J must be exceeded in order to have transmission. Such a result is not surprising since the linear transmission is unstable when E is in the energy gap, and it happens that the nonlinearity with $\lambda>0$ stabilizes it for E below -2, while enhancing the instability when E above 2 (reverse situation occurs for $\lambda<0$, i.e., for the holes). In Fig. 5(d) we plot the electron probability density r_n^2 as a function of the sample length for the state associated with the chaotic orbit around the period-2 hyperbolic orbit [see Fig. 5(c)]. Such chaotic states will certainly generate noisy responses in the transmission process, induced by fluctuations in the values of the parameters of the system such as E or k, which are affected by the potential difference across the interfaces between the nonlinear sample and linear leads, as well as the sample length N. To show the latter, we plot in Fig. 6 the "power spectral density" for the serial values of the transmission

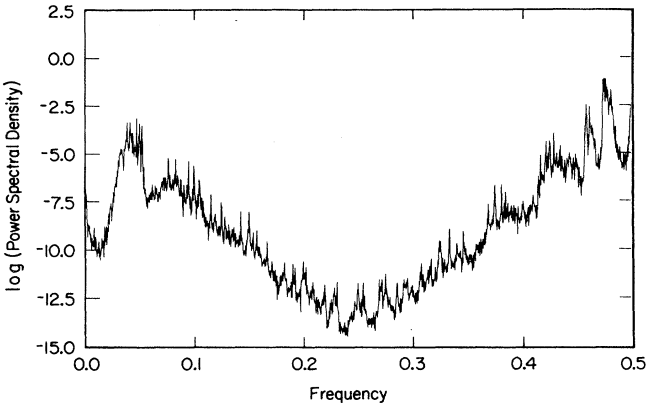

FIG. 6. Logarithmic "power spectral density" of a series of values of the transmission coefficient as function of the nonlinear sample length, $t(N)$, for the chaotic state at $E=-1.0$ and $T^2=1.0593$, corresponding to the chaotic orbit around the period-2 hyperbolic orbit in Fig. 5(c).

coefficient, $t(N)$, corresponding to the above-mentioned chaotic state. The spectra are the superposition of those from the noisy component and the underlying quasiperiodic components, where two prominent peaks in the envelope centered at frequencies $f\sim 0.5$ and ~ 0.05 are due to the quasiperiodic structures in the orbit surrounding the period-2 hyperbolic orbit. In fact, this orbit alternates between the basins of the period-2 elliptic orbit [Fig. 5(c)], and also appears as repeated groups [Fig. 5(d)], giving rise to responses at the above-mentioned frequencies, respectively. Finally, we note that in the above analyses T^2 is used as variable to measure the magnitude of nonlinearity. Alternatively, one can discuss the transmission properties by varying the Fermi level E while keeping T constant. In view of the "phase diagram," one can expect similar qualitative results in that case.

In conclusion, we have systematically studied the effects of nonlinearity on the transmission of waves in one-dimensional periodic lattices described by the tight-binding Hamiltonian. The mechanism for the bistability or multistability induced by the nonlinear periodic medium can be well studied by analysis of an area-preserving nonlinear mapping. The transmission coefficient exhibits plateaus as a function of the incident intensity, due to the presence of transmission gaps. We have shown the phase diagram of the transmission problem in terms of energy E and nonlinear coupling constant λ, which has very interesting structure. This structure is well understood in our analysis of the nonlinear mapping. We have also found that when such a nonlinear medium is illuminated with radiation of well-defined energy in the gap of the periodic system, increasing the incident power can switch it from a state of low transmissivity to a state with transmission coefficient equal to 1. Finally, the noisy nonlinear responses belong to the category of deterministic noise and would appear as intrinsic and reproducible effects of the physical system. Our nonlinear system thus yields a new mechanism for generation of noise. It will be very interesting to check these theoretical results experimentally. On the other hand, we have studied here only the much simplified physical model. It is our intention to study these properties in more realistic physical systems in the future.

ACKNOWLEDGMENTS

Ames Laboratory is operated for the U.S. Department of Energy (DOE) by Iowa State University under Contract No. W-7405-ENG-82. This investigation was supported by the Director for Energy Research, Office of Basic Energy Sciences, U.S. DOE. This work was partially supported by North Atlantic Treaty Organization Grant No. RG674/88.

[1]T. D. Holstein, Ann. Phys. (N.Y.) **8**, 325 (1959); L. A. Turkevich and T. D. Holstein, Phys. Rev. B **35**, 7474 (1987).
[2]Morrel H. Cohen, E. N. Economou, and C. M. Soukoulis, Phys. Rev. Lett. **51**, 1202 (1983).
[3]Wei Chen and D. L. Mills, Phys. Rev. Lett. **58**, 160 (1987).
[4]A. A. Abrikosov, A. I. Buzdin, and M. L. Kulić, Supercond. Sci. Technol. **1**, 260 (1989).
[5]Per Bak, Rep. Prog. Phys. **45**, 587 (1982).
[6]A. J. Lichtenberg and M. A. Lieberman, *Regular and Stochastic Motion* (Springer-Verlag, New York, 1983).
[7]V. I. Arnold and A. Avez, *Ergodic Problems of Classical Mechanics* (Benjamin, New York, 1968).
[8]M. V. Berry, in *Topics in Nonlinear Dynamics (La Jolla Institute)* Proceedings of the Workshop on Topics in Nonlinear Dynamics, AIP Conf. Proc. No. 46, edited by S. Jorna (AIP, New York, 1978).
[9]B. V. Chirikov, Phys. Rep. **52**, 263, (1979).
[10]R. H. G. Helleman, in *Universality in Chaos,* edited by P. Cvitanović (Hilger, Bristol, 1984).
[11]J. M. Greene, J. Math. Phys. **20**, 1183 (1979).
[12]J. M. Greene, R. S. Mackay, F. Vivaldi, and M. J. Feigenbaum, Physica D **3**, 468 (1981).
[13]James D. Meiss, Phys. Rev. A **34**, 2375 (1986).
[14]Yi Wan and C. M. Soukoulis, Phys. Rev. A (to be published).
[15]Volker Heine, Phys. Rev. **138**, A1689 (1965).
[16]David Allender, James Bray, and John Bardeen, Phys. Rev. B **7**, 1020 (1973).
[17]F. Delyon, Y. E. Levy, and B. Souillard, Phys. Rev. Lett. **57**, 2010 (1986).
[18]L. Kahn, N. S. Almeida, and D. L. Mills, Phys. Rev. B **37**, 8072 (1988).
[19]T. C. Bountis, C. R. Eminhizer, and R. H. G. Helleman, in *Long-Time Prediction in Dynamics,* edited by C. W. Horton, Jr., L. E. Reichl, and V. G. Szebehely (Wiley, New York, 1983).